

The dynamics of starvation and recovery

2 Justin D. Yeakel * †‡, Christopher P. Kempes †, and Sidney Redner †§

3 *School of Natural Science, University of California Merced, Merced, CA, †The Santa Fe Institute, Santa Fe, NM, §Department of Physics, Boston University, Boston
4 MA, and ‡To whom correspondence should be addressed: jdyeakel@gmail.com

5 Submitted to Proceedings of the National Academy of Sciences of the United States of America

6 The eco-evolutionary dynamics of species is fundamentally linked
7 to the energetic constraints of its constituent individuals. Of par-
8 ticular importance are the tradeoffs between reproduction and
9 the dynamics of starvation and recovery in resource-limited envi-
10 ronments. To elucidate the consequences of this tradeoff, we
11 introduce a minimal nutritional state-structured model that in-
12 corporates two classes of consumer: nutritionally replete con-
13 sumers that reproduce, and undernourished, non-reproducing
14 consumers that are susceptible to mortality. As a function of the
15 transition rates between these replete and undernourished states
16 that are determined by the presence or absence of resources,
17 the consumer populations can either undergo cyclic dynamics or
18 reach a steady state. We obtain strong constraints on starvation
19 and recovery rates by deriving allometric scaling relationships
20 and find that population dynamics subject to these constraints
21 can approach the cyclic regime but are typically driven to a steady
22 state. Moreover, we find these rates fall within a ‘refuge’ in pa-
23 rameter space, where the probability of extinction of the consumer
24 population is minimized. Thus we identify a potential mechanism
25 that may both drive and constrain the dynamics of animal pop-
26ulations. Our model provides a natural framework that predicts
27 maximum body size for mammals by determining the relative sta-
28 bility of an otherwise homogeneous population to a mutant pop-
29 ulation with altered percent body fat. For body masses $\lesssim 10^6$ g,
30 a more apidose invader dominates over the resident population,
31 and vice versa for body mass $\gtrsim 10^6$ g, thus providing a principled
32 mechanism for a within-lineage driver of Cope’s rule.

33 foraging | starvation | reproduction

34 Introduction

35 The behavioral ecology of nearly all organisms is influenced by
36 the energetic state of individuals, which directly influences how
37 they invest reserves in uncertain environments. Such behav-
38 iors are generally manifested as tradeoffs between investing in
39 somatic maintenance and growth, or allocating energy towards
40 reproduction [1, 2, 3]. The timing of these behaviors responds
41 to selective pressure, as the choice of the investment impacts
42 future fitness [4]. The influence of resource limitation on an
43 organism’s ability to maintain its nutritional stores may lead to
44 repeated delays or shifts in reproduction over the course of an
45 organism’s life.

46 The balance between (a) somatic growth and maintenance,
47 and (b) reproduction is often conditioned on resource availabil-
48 ity [5]. For example, reindeer invest less in calves born after
49 harsh winters (when the mother’s energetic state is depleted)
50 than in calves born after moderate winters [6]. Many bird
51 species invest differently in broods during periods of resource
52 scarcity compared to normal periods [7, 8], sometimes delaying
53 or even foregoing reproduction for a breeding season [1, 9, 10].
54 Even freshwater and marine zooplankton have been observed to
55 avoid reproduction under nutritional stress [11], and those that
56 do reproduce have lower survival rates [2]. Organisms may also
57 separate maintenance and growth from reproduction over space
58 and time: many salmonids, birds, and some mammals return to
59 migratory breeding grounds to reproduce after one or multiple
60 seasons in resource-rich environments where they accumulate
61 nutritional reserves [12, 13, 14].

62 Physiology also plays an important role in regulating re-
63 productive expenditures during periods of resource limitation.
64 The data collected thus far has shown that diverse mammals (47

65 species in 10 families) exhibit delayed implantation, whereby fe-
66 males postpone fetal development (blastocyst implantation) un-
67 til nutritional reserves can be accumulated [15, 16]. Many other
68 many species (including humans) suffer irregular menstrual cy-
69 cling and higher spontaneous abortion rates during periods of
70 nutritional stress [17, 18]. In the extreme case of unicellular
71 organisms, nutrition is unavoidably linked to reproduction be-
72 cause the nutritional state of the cell regulates all aspects of the
73 cell cycle [19]. The existence of so many independently evolved
74 mechanisms across such a diverse suite of organisms highlights
75 the importance and universality of the fundamental tradeoff
76 between somatic and reproductive investment. However the
77 dynamic implications of these constraints are unknown.

78 Though straightforward conceptually, incorporating the en-
79 ergetic dynamics of individuals [20] into a population-level
80 framework [20, 21] presents numerous mathematical obsta-
81 cles [22]. An alternative approach involves modeling the
82 macroscale relations that guide somatic versus reproductive
83 investment in a consumer-resource system. For example,
84 macroscale Lotka-Volterra models assume that the growth rate
85 of the consumer population depends on resource density, thus
86 implicitly incorporating the requirement of resource availability
87 for reproduction [23].

88 In this work, we adopt an alternative approach in which we
89 explicitly account for resource limitation and the subsequent
90 effect of starvation. Namely, only individuals with sufficient en-
91 ergetic reserves can reproduce. Such a constraint leads to repro-
92 ductive time lags due to some members of the population going
93 hungry and then recovering. Additionally, we incorporate the
94 idea that reproduction is strongly constrained allometrically[3],
95 and is not generally linearly related to resource density. As we
96 shall show, these constraints influence the ensuing population
97 dynamics in dramatic ways.

98 **99 Nutritional state-structured model (NSM)**
100 We begin by defining a minimal Nutritional State-structured
101 population Model (NSM), where the consumer population is
102 partitioned into two states: (a) an energetically replete (full)
103 state F , where the consumer reproduces at a constant rate λ
104 and does not die from starvation, and (b) an energetically de-
105 ficient (hungry) state H , where the consumer does not repro-
106 duce but dies by starvation at rate μ . The underlying resource
107 R evolves by logistic growth with an intrinsic growth rate α
108 and a carrying capacity equal to one. Consumers transition
109 from the full state F to the hungry state H at a rate σ —the

Reserved for Publication Footnotes

starvation rate—and also in proportion to the absence of re-
 sources ($1 - R$). Conversely, consumers recover from state H to state F at rate ρ and in proportion to R . Resources are also eaten by the consumers—at rate ρ by hungry consumers and at rate $\beta < \rho$ by full consumers. This inequality accounts for hungry consumers requiring more resources to replace lost body tissue. The NSM represents a fundamental extension of the idealized starving random walk model of foraging, which focuses on resource depletion, to include reproduction and source replenishment [24, 25, 26].

In the mean-field approximation, in which the consumers and resources are perfectly mixed, their densities evolve according to the rate equations

$$\begin{aligned}\dot{F} &= \lambda F + \rho RH - \sigma(1 - R)F, \\ \dot{H} &= \sigma(1 - R)F - \rho RH - \mu H, \\ \dot{R} &= \alpha R(1 - R) - R(\rho H + \beta F).\end{aligned}$$

Notice that the total consumer density $F + H$ evolves according to $\dot{F} + \dot{H} = \lambda F - \mu H$. This resembles the equation of motion for the predator density in the classic Lotka-Volterra model [27], except that the resource density does not appear in the growth term. As discussed above, the attributes of reproduction and mortality have been explicitly apportioned to the full and hungry consumers, respectively, so that the growth in the total density is decoupled from the resource density.

Equation [1] has three fixed points: two trivial fixed points at $(F^*, H^*, R^*) = (0, 0, 0)$ and $(0, 0, 1)$, and one non-trivial, internal fixed point at

$$\begin{aligned}F^* &= \frac{\alpha\lambda\mu(\mu + \rho)}{(\lambda\rho + \mu\sigma)(\lambda\rho + \mu\beta)}, \\ H^* &= \frac{\alpha\lambda^2(\mu + \rho)}{(\lambda\rho + \mu\sigma)(\lambda\rho + \mu\beta)}, \\ R^* &= \frac{\mu(\sigma - \lambda)}{\lambda\rho + \mu\sigma}.\end{aligned}$$

The stability of this fixed point is determined by the Jacobian matrix \mathbf{J} , where each matrix element $J_{ij} = \partial\dot{X}_i/\partial X_j$ when evaluated at the internal fixed point, and \mathbf{X} is the vector (F, H, R) . The parameters in Eq. [1] are such that the real part of the largest eigenvalue of \mathbf{J} is negative, so that the system is stable with respect to small perturbations from the fixed point. Because this fixed point is unique, it is the global attractor for all population trajectories for any initial condition where the resource and consumer densities are both nonzero.

From Eq. [2], an obvious constraint on the NSM is that the reproduction rate λ must be less than the starvation rate σ , so that R^* is positive. In fact, when the resource density $R = 0$, the rate equation for F gives exponential growth of F for $\lambda > \sigma$. The condition $\sigma = \lambda$ represents a transcritical (TC) bifurcation [28] that demarcates the physical regime from the unphysical regime where F would grow exponentially with time. The biological implication of the constraint $\lambda < \sigma$ has a simple interpretation—the rate at which a macroscopic organism loses mass due to lack of resources is generally much faster than the rate of reproduction. As we will discuss below, this inequality is a natural consequence of allometric constraints [3] for organisms within empirically observed body size ranges (Fig. 2).

In the physical regime of $\lambda < \sigma$, the fixed point [2] may either be a stable node or a limit cycle (Fig. 3). In continuous-time systems, a limit cycle arises when a pair of complex conjugate eigenvalues crosses the imaginary axis to attain positive real parts [29]. This Hopf bifurcation is defined by $\text{Det}(\mathbf{S}) = 0$, with \mathbf{S} the Sylvester matrix, which is composed of the coefficients of the characteristic polynomial of the Jacobian ma-

stable regime but close to the Hopf bifurcation, the amplitude of the transient but decaying cycles become large. Given that logical systems are constantly being perturbed [31], the onset of transient cycles, even though they decay with time in the mean-field description, can increase the extinction risk [32, 33, 34]. Thus the distance of a system from the Hopf bifurcation vides a measure of its persistence.

When the starvation rate $\sigma \gg \lambda$, a substantial fraction of the consumers are driven to the hungry non-reproducing state. Because reproduction is inhibited, there is a low steady-state consumer density and a high steady-state resource density. However, if $\sigma/\lambda \rightarrow 1$ from above, the population is overloaded with energetically-replete (reproducing) individuals, thereby promoting oscillations between the consumer and resource densities (Fig. 3).

Whereas the relation between consumer growth rate λ and the starvation rate σ defines an absolute bound of biological feasibility—the TC bifurcation— σ also determines the sensitivity of the consumer population to changes in resource density. When $\sigma \gg \lambda$, the steady-state population density is small, thereby increasing the risk of stochastic extinction. On the other hand, as σ decreases, the system will ultimately be poised either near the TC or the Hopf bifurcation (Fig. 3). If the recovery rate ρ is sufficiently small, the TC bifurcation is reached and the resource eventually is eliminated. If ρ exceeds a threshold value, cyclic dynamics will develop as the Hopf bifurcation is approached.

Role of allometry

While there are no a priori constraints on the parameters in the NSM, most organisms correspond to restricted portions of the parameter space. Here we use allometric scaling relations to constrain the covariation of rates in a principled and biologically meaningful manner. Allometric scaling relations highlight common constraints and average trends across large ranges in body size and species diversity. Many of these relations can be derived from a small set of assumptions and below we describe a

framework to determine the covariation of timescales and rates across the range of mammals for each of the key parameters of our model (cf. [35]). We are thereby able to define the regime of dynamics occupied by the entire class of mammals along with the key differences between the largest and smallest mammals.

Nearly all of the rates described in the NSM are determined by consumer metabolism, which can be used to describe a variety of organismal features [36]. The scaling relation between an organism's metabolic rate B and its body mass M at reproductive maturity is known to scale as $B = B_0 M^\eta$ [37], where the scaling exponent η is typically close to $2/3$ or $3/4$ for metazoans (e.g., [36]), and has taxonomic shifts for unicellular species between $\eta \approx 1$ in eukaryotes and $\eta \approx 1.76$ in bacteria [38, 3]. An organism's metabolic rate B is proportional to the cost of tissue maintenance in the absence of growth (i.e., when the body mass is M). By definition $B = \beta/\xi$, where β is the rate at which resources are consumed for full consumers (see Eq. [1]) and where ξ is related to the conversion efficiency of resource to consumer tissue (Supporting Information, section XX).

Several efforts have shown how a partitioning of B between growth and maintenance purposes can be used to derive a general equation for both the growth trajectories and growth rates of organisms ranging from bacteria to metazoans [39, 40, 41, 42, 3]. This relation is derived from the simple balance condition [39, 40, 41, 42, 3]

$$B_0 m^\eta = E_m \dot{m} + B_m m, \quad [3]$$

222 m is the mass of the organism at any point in its development. 272 synthesis a unit of biomass [42]. Given the replete mass, M ,
 223 This balance has the general solution [?, 3] 273 of an organism, the above energy balance prescribes the mass
 274 trajectory of a non-consuming organism:

$$\left(\frac{m(t)}{M}\right)^{1-\eta} = 1 - \left[1 - \left(\frac{m_0}{M}\right)^{1-\eta}\right] e^{-a(1-\eta)t/M^{1-\eta}} \quad [4]$$

$$m(t) = M e^{-a' t/M^{1-\eta}}. \quad [9]$$

224 where, for $\eta < 1$, $M = (B_0/B_m)^{1/(1-\eta)}$ is the asymptotic mass, 275 The time scale for starvation is given by the time it takes $m(t)$
 225 $a = B_0/E_m$, and m_0 is mass at birth. We now use this solution 276 to reach $\epsilon_\sigma M$, which gives
 226 to define the timescale (see [40] for a detailed presentation of
 227 these timescales) of reproduction and recovery from starvation.
 228 The time that it takes to reach a particular mass ϵM is given
 229 by the timescale

$$\tau(\epsilon) = \ln \left[\frac{1 - (m_0/M)^{1-\eta}}{1 - \epsilon^{1-\eta}} \right] \frac{M^{1-\eta}}{a(1-\eta)} \quad [5]$$

230 where we will define values of ϵ to describe a set of rates within
 231 our model. For the time to reproduce, $t_\lambda = \tau(\epsilon_\lambda)$, where ϵ_λ is
 232 the fraction of the asymptotic mass where an organism is repro-
 233 ductively mature and should be close to one (typically $\epsilon_\lambda \approx 0.95$
 234 [39]). The growth rate is then given by $\lambda = \ln(v)/t_\lambda$ where
 235 v is the number of offspring produced (see supplement), and
 236 for any constant value of ϵ_λ this will scale like $\lambda \propto M^{\eta-1}$ for
 237 $M \gg m_0$ [39, 40, 41, 42, 3].

238 The rate of recovery $\rho = 1/t_\rho$ requires that an organism
 239 accrues sufficient tissue to transition from the hungry to the
 240 full state. Since only certain tissues can be digested for energy
 241 (for example the brain cannot be degraded to fuel metabolism),
 242 we define the rates for starvation, death, and recovery by the
 243 timescales required to reach, or return from, specific fractions
 244 of the replete-state mass (see the Supporting Information for
 245 details on these parameterizations). We define $m_\sigma = \epsilon_\sigma M$,
 246 where $\epsilon_\sigma < 1$ is the fraction of replete-state mass where repro-
 247 duction ceases. This fraction will be modified if tissue com-
 248 position systematically scales with adult mass. For example,
 249 making use of the observation that body fat in mammals scales
 250 with overall body size according to $M_{\text{fat}} = f_0 M^\gamma$ and assum-
 251 ing that once this mass is fully digested the organism starves,
 252 this would imply that $\epsilon_\sigma = 1 - f_0 M^\gamma / M$. It follows that the
 253 recovery timescale, t_ρ , is the time to go from $m = \epsilon_\sigma \epsilon_\lambda M$ to
 254 $m = \epsilon_\lambda M$. Using Eqs. [4] and [5] this timescale is given by
 255 simply considering an adjusted starting mass of $m'_0 = \epsilon_\sigma \epsilon_\lambda M$,
 256 in which case

$$t_\rho = \ln \left[\frac{1 - (\epsilon_\sigma \epsilon_\lambda)^{1-\eta}}{1 - \epsilon^{1-\eta}} \right] \frac{M^{1-\eta}}{a'(1-\eta)} \quad [6]$$

257 where a' accounts for possible deviations in the biosynthetic en-
 258 ergetics during recovery (see Supporting Information). It should
 259 be noted that more complicated ontogenetic models explicitly
 260 handle storage [42], whereas this feature is implicitly covered
 261 by the body fat scaling in our framework.

262 To determine the starvation rate, σ , we are interested in the
 263 time required for an organism to go from a mature adult that
 264 reproduces at rate λ , to a reduced-mass hungry state where re-
 265 production is impossible. For starving individuals we assume
 266 that an organism must meet its maintenance requirements using
 267 the digestion of existing mass as the sole energy source. This
 268 assumption implies the following simple metabolic balance

$$\dot{m}E'_m = -B_m m \quad [7]$$

269 or

$$\dot{m} = -\frac{a'}{M^{1-\eta}} m \quad [8]$$

270 where E'_m is the amount of energy stored in a unit of exist-
 271 ing body mass which differs from E_m , the energy required to

302 **Stabilizing effects of allometric constraints**
 303 As the allometric derivations of the NSM rate laws reveal, star-
 304 vation and recovery rates are not independent parameters, and
 305 the biologically relevant portion of the phase space shown in
 306 Fig. 3 is constrained via covarying parameters. Given the pa-
 307 rameters of terrestrial endotherms, we find that σ and ρ are
 308 constrained to lie within a small window of potential values
 309 (Fig. 4) for the known range of body sizes M . We thus find
 310 that the dynamics for all mammalian body sizes is confined to
 311 the steady-state regime of the NSM and that limit-cycle behav-
 312 ior is precluded. Moreover, for larger M , the distance to the
 313 Hopf bifurcation increases, while uncertainty in allometric pa-
 314 rameters (20% variation around the mean; Fig. 4) results in
 315 little qualitative difference in the distance to the the Hopf bi-
 316 furcation. These results suggest that small mammals are more
 317 prone to population oscillations—both stable limit cycles and
 318 transient cycles—than mammals with larger body size. Thus
 319 our NSM model predicts that population cycles should be less
 320 common for larger species and more common for smaller species,
 321 particularly in environments where resources are limiting.

322 **[I don't see the point of the paragraph below.]** Pre-
 323 vious studies have used allometric constraints to explain the
 324 periodicity of cyclic populations [44, 45, 46], suggesting a pe-
 325 riod $\propto M^{0.25}$. However this relation seems to hold only for
 326 some species [47], and potential drivers range from predator
 327 and/or prey lifespans to competitive dynamics [48, 49]. Sta-
 328 tistically significant support for the existence of population cy-
 329 cles among mammals is predominantly based on time series for

330 small mammals [50], where our model would predict more pro-
331 nounced transient dynamics, given how close these points are to
332 the Hopf bifurcation. On the other hand, the longer gestational
333 times and the increased difficulty in measurements, precludes
334 obtaining similar-quality data for larger organisms.

335 Extinction risk

336 Within our model, higher rates of starvation result in a larger
337 flux of the population to the hungry state. In this state re-
338 production is absent, thus increasing the likelihood of extinc-
339 tion. From the perspective of population survival, it is the rate
340 of starvation relative to the rate of recovery that determines
341 the long-term dynamics of the various species (Fig. 3). We
342 therefore examine the competing effects of cyclic dynamics vs.
343 changes in steady state density on extinction risk as a function
344 of the ratio σ/ρ . To this end, we computed the probability of ex-
345 tinction, where we define extinction as a population trajectory
346 falling below one fifth of the allometrically constrained steady
347 state at any time between 10^6 and $\leq 10^8$. This procedure is re-
348 peated for 1000 replicates of the continuous-time system shown
349 in Eq. 1 for an organism of $M = 100$ grams. In each repli-
350 cate the initial densities are chosen to be $A(F^*, H^*, R^*)$, with
351 A a random variable that is uniformly distributed in $[0, 2]$. By
352 allowing the rate of starvation to vary, we assessed extinction
353 risk across a range of values of σ/ρ between ca. 10^{-3} to 5, thus
354 examining a horizontal cross-section of Fig. 3. As expected,
355 higher rates of extinction correlate with both low and high val-
356 ues of σ/ρ . For low values of σ/ρ , the increased extinction
357 risk results from transient cycles with larger amplitudes as the
358 system nears the Hopf bifurcation (Fig. 5). For large values
359 of σ/ρ , higher extinction risk arises because of the decrease in
360 the steady state consumer population density. This interplay
361 creates an ‘extinction refuge’ as shown in Fig. 5, such that for
362 a constrained range of σ/ρ , extinction probabilities are mini-
363 mized.

364 We find that the allometrically constrained values of σ/ρ
365 (with 20% variability around energetic parameter means) fall
366 within the extinction refuge. These values are close enough to
367 the Hopf bifurcation to avoid low steady state densities, and
368 far enough away to avoid large-amplitude transient cycles. The
369 fact that allometric values of σ and ρ fall within this relatively
370 small window supports the possibility that a selective mech-
371 anism has constrained the physiological conditions that drive
372 starvation and recovery rates within populations. Such a mech-
373 anism would select for organism physiology that generates ap-
374 propriate σ and ρ values that avoid extinction. This selection
375 could occur via the tuning of body fat percentages, metabolic
376 rates, and biomass maintenance efficiencies. To summarize,
377 our finding that the allometrically-determined parameters fall
378 within this low extinction probability region suggests that the
379 NSM dynamics may both drive—and constrain—natural ani-
380 mal populations.

381 Dynamic and energetic barriers to body size

382 Metabolite transport constraints are widely thought to place
383 strict boundaries on biological scaling [51, 52, 36] and thereby
384 lead to specific predictions on the minimum possible body size
385 for organisms [53]. Above this bound, a number of energetic and
386 evolutionary mechanisms have been explored to assess the costs
387 and benefits associated with larger body masses, particularly
388 for mammals. One important such example is the *fasting en-*
389 *durance hypothesis*, which contends that larger body size, with
390 consequent lower metabolic rates and increased ability to main-
391 tain more endogenous energetic reserves, may buffer organisms
392 against environmental fluctuations in resource availability [54].
393 Over evolutionary time, terrestrial mammalian lineages show a

394 significant trend towards larger body size (known as Cope’s
395 Rule) [55, 56, 57, 58], and it is thought that within-lineage
396 drivers generate selection towards an optimal upper bound of
397 roughly 10^7 grams [55], whose value may arise from higher ex-
398 tinction risk for large taxa over evolutionary timescales [56].

399 These trends are thought to be driven by a combination of
400 climate change and niche availability [58]; however the under-
401 pinning energetic costs and benefits of larger body sizes, and
402 how they influence dynamics over ecological timescales, have
403 not been explored. We argue that the NSM provides a suitable
404 framework to explore these issues.

405 The NSM correctly predicts that species with smaller
406 masses have larger steady-state population densities (Fig. 6a).
407 It should also be noted that R^* is decreasing for increasing
408 body size. From the perspective of classic resource competition
409 theory we would expect that the species that can live on the
410 lowest resource abundance should outcompete others [?, ?, ?].
411 The NSM then predicts that larger mammals should outcom-
412 pete smaller ones, supporting Cope’s rule. This is a natural
413 consequence of the steady-state dynamics combined with the
414 derived timescales.

415 Furthermore, many previous studies have focused on the en-
416 ergy equivalence hypothesis which argues that the total energy
417 use, B_{tot} , of a population is constant independent of species
418 size (e.g. [?, ?]). This hypothesis is based on observations
419 showing that the abundance, N , of a species is proportional to
420 the inverse of individual metabolism (e.g. $N \propto M^{-3/4}/B_0$)
421 (e.g. [?, ?]). This is usually stated as $B_{tot} = NB = \text{constant}$
422 which has been shown to hold in mammalian and vascular plant
423 communities (e.g. [?, ?]). Figure ?? shows that both F^* and
424 H^* scale like $M^{-\eta}$ over a wide range of organism sizes and
425 Figure ?? shows that F^*B is a constant over this same range.
426 This result is remarkable because it illustrates that the steady
427 state values of the NSM combined with the derived timescales
428 naturally give rise to the energy equivalence result. Further-
429 more, the equivalence breaks down at distinct sizes at both
430 the large and small end of mammals suggesting that these are
431 hard limits on mammalian body sizes because organisms out-
432 side this range do not meet the constant efficiency obeyed by
433 other populations. Significant deviations from constant energy
434 use occur at *Justin – VALUE* at the small end of mammals
435 and *Justin – VALUE* for the large end. Compellingly, this
436 dynamic bound, which is determined by the rate of energetic
437 recovery, is close to the minimum observed mammalian body
438 size of ca. 1.3–2.5 grams (Fig. 6b,c), a range that occurs as the
439 recovery rate begins its decline. In addition to known trans-
440 port limitations [53], we suggest that an additional constraint
441 of lower body size stems from the dynamics of starvation. This
442 result mirrors other efforts [3, ?] where at a given scale multiple
443 limitations constrain the smallest possibilities for life within a
444 class of organisms.

445 A additional theoretical upper bound on mammalian body
446 size is given by $\epsilon = 0$, where mammals are entirely composed of
447 metabolic reserves, and this occurs at a size of $M = 8.3 \times 10^8$,
448 or $4.5 \times$ the mass of a blue whale. We determine a more real-
449 istic upper bound to body mass by assessing the susceptibility
450 of an otherwise homogeneous population to invasion by a mu-
451 tated subset of the population (denoted by χ) where individuals
452 have a modified proportion of body fat $M' = M(1 + \chi)$ where
453 $\chi \in [-0.5, 0.5]$, thus altering the rates of starvation σ , recov-
454 ery ρ , and maintenance β . There is no internal fixed point
455 that correspond to a state where both original residents and
456 invaders coexist (except for the trivial state $\chi = 0$). To assess
457 the susceptibility to invasion as a function of the invader mass,
458 we determine which consumer has a higher steady-state den-
459 sity for a given value of χ . We find that for $1 \leq M < 10^6$ g,
460 having additional body fat ($\chi > 0$) results in a higher steady-

462 state invader population density ($H'^* + F'^* > H^* + F^*$). Thus 488 mammals [59, 60, 61] which were also much more geographi-
 463 the invader has an intrinsic advantage over the resident pop- 489 cally widespread than today. These results, combined with our
 464 ulation. However, for $M > 10^6$, leaner individuals ($\chi < 0$) 490 findings, suggest that the modern diversity of mammals may
 465 have the advantage, and this is due to the changing covariance 491 not represent a true steady state the current distribution of
 466 between energetic rates as a function of modified energetic re- 492 nutrients and large seeds may be very different from the past
 467 serves [I don't understand the phrase after the comma 493 [59, 60, 61].
 468 AND STILL DON'T].

469 The observed switch in susceptibility as a function of χ 494 The energetics associated with somatic maintenance,
 470 at $M_{\text{opt}} \approx 10^6$ thus serves as an attractor, where over evo- 495 growth, and reproduction are important elements that influence
 471 lutionary time the NSM predicts organismal mass to increase 496 the dynamics of all populations [9]. The NSM is a minimal and
 472 if $M < M_{\text{opt}}$ and decrease if $M > M_{\text{opt}}$. Moreover, M_{opt} , 497 general model that incorporates the dynamics of starvation that
 473 which is entirely determined by the population-level conse- 498 are expected to occur in resource-limited environments. By in-
 474 quences of energetic constraints, is within an order of magnitude 499 corporating allometric relations between the rates in the NSM,
 475 of the mass observed in the North American mammalian fossil 500 we found: (i) different organismal masses have distinct popu-
 476 record [55] and also the mass predicted from an evolutionary 501 lation dynamic regimes, (ii) allometrically-determined rates of
 477 model of body size evolution [56]. While the state of the envi- 502 starvation and recovery appear to minimize extinction risk, and
 478 ronment, as well as the competitive landscape, will determine 503 (iii) the dynamic consequences of these rates may place addi-
 479 whether specific body sizes are selected for or against [58], we 504 tional barriers on the evolution of minimum and maximum body
 480 suggest that the starvation dynamics outlined here may pro- 505 size. We suggest that the NSM offers a means by which the dy-
 481 vide the driving mechanism for the evolution of larger body 506 namic consequences of energetic constraints can be assessed us-
 482 size among terrestrial mammals. 507 ing macroscale interactions between and among species. Future
 483 One might be concerned a greater number of large mam- 508 efforts will involve exploring the consequences of these dynamics
 484 mals are currently not observed in the modern world given that 509 in a spatially explicit framework, thus incorporating elements
 485 larger mammals are less susceptible to extinction. However, 510 such as movement costs and spatial heterogeneity, which may
 486 recent research suggests that the pleistocene may have been 511 elucidate additional tradeoffs associated with the dynamics of
 487 much more populated with a significant diversity of very large 512 starvation.

- 513 1. Martin TE (1987) Food as a Limit on Breeding Birds: A Life-History Perspective. *Annu. Rev. Ecol. Syst.* 18:453–487.
- 514 2. Kirk KL (1997) Life-History Responses to Variable Environments: Starvation and 560 24. Bénichou O, Redner S (2014) Depletion-controlled starvation of a diffusing forager. *Phys. Rev. Lett.* 113:238101.
- 515 Reproduction in Planktonic Rotifers. *Ecology* 78:434–441.
- 516 25. Bénichou O, Chupeau M, Redner S (2016) Role of Depletion on the Dynamics of a 561 Diffusing Forager. *ArXiv e-prints*.
- 517 3. Kempes CP, Dutkiewicz S, Follows MJ (2012) Growth, metabolic partitioning, and 562 26. Chupeau M, Bénichou O, Redner S (2016) Universality classes of foraging with 563 the size of microorganisms. *PNAS* 109:495–500.
- 518 564 27. Murray JD (2002) *Mathematical Biology I. An Introduction* (3rd ed.) (Springer-Verlag 565 Berlin, 2002).
- 519 4. Mangel M, Clark CW (1988) *Dynamic Modeling in Behavioral Ecology* (Princeton 566 28. Strogatz SH (2014) *Nonlinear Dynamics and Chaos: With Applications to Physics, 567 Biology, Chemistry, and Engineering* (2nd ed.) (Westview Press, 2014).
- 520 University Press, Princeton).
- 521 5. Morris DW (1987) Optimal Allocation of Parental Investment. *Oikos* 49:332.
- 522 6. Tveraa T, Fauchald P, Henaug C, Yoccoz NG (2003) An examination of a com- 567 29. Guckenheimer J, Holmes P (1983) *Nonlinear oscillations, dynamical systems, and 568 bifurcations of vector fields* (Springer, New York).
- 523 pensatory relationship between food limitation and predation in semi-domestic 569 30. Gross T, Feudel U (2004) Analytical search for bifurcation surfaces in parameter 570 reindeer. *Oecologia* 137:370–376.
- 524 571 31. Hastings A (2001) Transient dynamics and persistence of ecological systems. *Ecol. 572 Lett.* 4:215–220.
- 525 7. Daan S, Dijkstra C, Drent R, Meijer T (1988) *Food supply and the annual timing of 573 avian reproduction*.
- 526 8. Jacot A, Valcu M, van Oers K, Kempenaers B (2009) Experimental nest site lim- 574 32. Neubert M, Caswell H (1997) Alternatives to resilience for measuring the responses 575 itation affects reproductive strategies and parental investment in a hole-nesting 576 of ecological systems to perturbations. *Ecology* 78:653–665.
- 527 passerine. *Animal Behaviour* 77:1075–1083.
- 528 577 33. Caswell H, Neubert MG (2005) Reactivity and transient dynamics of discrete-time 578 34. Neubert M, Caswell H (2009) Detecting reactivity. *Ecology* 90:2683–2688.
- 529 9. Stearns SC (1989) Trade-Offs in Life-History Evolution. *Funct. Ecol.* 3:259.
- 530 579 35. Yodzis P, Innes S (1992) Body Size and Consumer-Resource Dynamics. *Am. Nat.* 580 139:1151–1175.
- 531 10. Barboza P, Jorde D (2002) Intermittent fasting during winter and spring affects body 581 36. Brown J, Gillooly J, Allen A, Savage V, West G (2004) Toward a metabolic theory of 582 composition and reproduction of a migratory duck. *J Comp Physiol B* 172:419–434.
- 532 583 37. West GB, Woodruff WH, Brown JH (2002) Allometric scaling of metabolic rate from 584 molecules and mitochondria to cells and mammals. *Proc. Natl. Acad. Sci. USA* 99 585 Suppl 1:2473–2478.
- 533 11. Threlkeld ST (1976) Starvation and the size structure of zooplankton communities. 586 38. DeLong JP, Okie JG, Moses ME, Sibly RM, Brown JH (2010) Shifts in metabolic 587 Freshwater Biol. 6:489–496.
- 534 588 scaling, production, and efficiency across major evolutionary transitions of life. *PNAS* 107:12941–12945.
- 535 12. Weber TP, Ens BJ, Houston AI (1998) Optimal avian migration: A dynamic model 589 39. West GB, Brown JH, Enquist BJ (2001) A general model for ontogenetic growth. 590 of fuel stores and site use. *Evolutionary Ecology* 12:377–401.
- 536 591 40. Moses ME, et al. (2008) Revisiting a Model of Ontogenetic Growth: Estimating Model 592 Parameters from Theory and Data. <http://dx.doi.org.proxy.lib.sfu.ca/10.1086/679735>
- 537 13. Mduma SAR, Sinclair ARE, Hilborn R (1999) Food regulates the Serengeti wilde- 593 41. Gillooly JF, Charnov EL, West GB, Savage VM, Brown JH (2002) Effects of size and 594 beest: a 40-year record. *J. Anim. Ecol.* 68:1101–1122.
- 538 595 42. Hou C, et al. (2008) Energy Uptake and Allocation During Ontogeny. *Science* 596 322:736–739.
- 539 14. Moore JW, Yeakel JD, Peard D, Lough J, Beere M (2014) Life-history diversity and its 597 43. Folland JP, Mc Cauley TM, Williams AG (2008) Allometric scaling of strength mea- 598 importance to population stability and persistence of a migratory fish: steelhead 599 surements to body size. *Eur J Appl Physiol* 102:739–745.
- 540 in two large North American watersheds. *J. Anim. Ecol.* 83:1035–1046.
- 541 600 44. Calder III WA (1983) An allometric approach to population cycles of mammals. *J. 601 Theor. Biol.* 100:275–282.
- 542 15. Mead RA (1989) in *Carnivore Behavior, Ecology, and Evolution* (Springer US, 602 45. Peterson RO, PAGE RE, DODGE KM (1984) Wolves, Moose, and the Allometry of 603 Boston, MA), pp 437–464.
- 543 604 Population Cycles. *Science* 224:1350–1352.
- 544 16. Sandell M (1990) The Evolution of Seasonal Delayed Implantation. *The Quarterly 605 46. Kruckoski GS, Schaffer WM (1991) Population cycles in mammals and birds: Does 606 Review of Biology* 65:23–42.
- 545 607 periodicity scale with body size? *J. Theor. Biol.* 148:469–493.
- 546 17. Bulik CM, et al. (1999) Fertility and Reproduction in Women With Anorexia Nervosa. 608
- 547 *J. Clin. Psychiatry* 60:130–135.
- 548 18. Trites AW, Donnelly CP (2003) The decline of Steller sea lions *Eumetopias jubatus* 609
- 549 in Alaska: a review of the nutritional stress hypothesis. *Mammal Review* 33:3–28.
- 550 19. Glazier DS (2009) Metabolic level and size scaling of rates of respiration and growth 610
- 551 in unicellular organisms. *Funct. Ecol.* 23:963–968.
- 552 20. Kooijman SALM (2000) *Dynamic Energy and Mass Budgets in Biological Systems* 611
- 553 (Cambridge).
- 554 21. Sousa T, Domingos T, Poggiale JC, Kooijman SALM (2010) Dynamic energy budget 612
- 555 theory restores coherence in biology. *Philos. T. Roy. Soc. B* 365:3413–3428.
- 556 22. Diekmann O, Metz JAJ (2010) How to lift a model for individual behaviour to the 613 population level? *Philos. T. Roy. Soc. B* 365:3523–3530.
- 557 23. Murdoch WW, Briggs CJ, Nisbet RM (2003) *Consumer-resource Dynamics*, Mono- 614
- 558 graphs in population biology (Princeton University Press).
- 559 615

- 608 47. Hendriks AJ, Mulder C (2012) Delayed logistic and Rosenzweig(MacArthur models 630 57. Smith F, Boyer A, Brown J, Costa D (2010) The Evolution of Maximum Body Size of
 609 with allometric parameter setting estimate population cycles at lower trophic levels 631 Terrestrial Mammals. *Science*.
 610 well. *Ecological Complexity* 9:43–54.
- 611 48. Kendall BE, et al. (1999) Why do populations cycle? A synthesis of statistical and 632 58. Saarinen JJ, et al. (2014) Patterns of maximum body size evolution in Cenozoic
 612 mechanistic modeling approaches. *Ecology* 80:1789–1805. 633 land mammals: eco-evolutionary processes and abiotic forcing. *Proc Biol Sci*
 613 49. Höglstedt G, Seljal T, Breistol A (2005) Period length in cyclic animal populations. 634 281:20132049–20132049.
 614 *Ecology* 86:373–378.
- 615 50. Kendall, Prendergast, Bjornstad (1998) The macroecology of population dynamics: 635 59. Doughty CE, Wolf A, Malhi Y (2013) The legacy of the Pleistocene megafauna
 616 taxonomic and biogeographic patterns in population cycles. *Ecol. Lett.* 1:160–164. 636 extinctions on nutrient availability in Amazonia. *Nature Geosci* 6:761–764.
 617 51. Brown J, Marquet P, Taper M (1993) Evolution of body size: consequences of an 637 60. Doughty CE, et al. (2016) Megafauna extinction, tree species range reduction, and
 618 energetic definition of fitness. *Am. Nat.* 142:573–584. 638 carbon storage in Amazonian forests. *Ecography* 39:194–203.
 619 52. West GB, Brown JH, Enquist BJ (1997) A General Model for the Origin of Allometric 639 61. Doughty CE, Faurby S, Svenning JC (2016) The impact of the megafauna extinctions
 620 Scaling Laws in Biology. *Science* 276:122–126. 640 on savanna woody cover in South America. *Ecography* 39:213–222.
- 621 53. West GB, Woodruff WH, Brown JH (2002) Allometric scaling of metabolic rate from 641 **ACKNOWLEDGMENTS.** We thank Luis Bettancourt, Eric Libby, and Seth New-
 622 molecules and mitochondria to cells and mammals. *Proc. Natl. Acad. Sci. USA* 642 some for helpful discussions and comments on the manuscript. J.D.Y. was sup-
 623 99:2473–2478. 643 ported by startup funds at the University of California, Merced, and an Omidyar
 624 54. Millar J, Hickling G (1990) Fasting Endurance and the Evolution of Mammalian 644 Postdoctoral Fellowship at the Santa Fe Institute. C.P.K. was supported by an
 625 Body Size. *Funct. Ecol.* 4:5–12. 645 Omidyar Postdoctoral Fellowship at the Santa Fe Institute. S.R. was supported
 626 55. Alroy J (1998) Cope's rule and the dynamics of body mass evolution in North 646 by grants DMR-1608211 and 1623243 from the National Science Foundation,
 627 American fossil mammals. *Science* 280:731. 647 and by the John Templeton Foundation, all at the Santa Fe Institute.
- 628 56. Clauset A, Redner S (2009) Evolutionary Model of Species Body Mass Diversifica- 648
 629 tion. *Phys. Rev. Lett.* 102:038103. 649

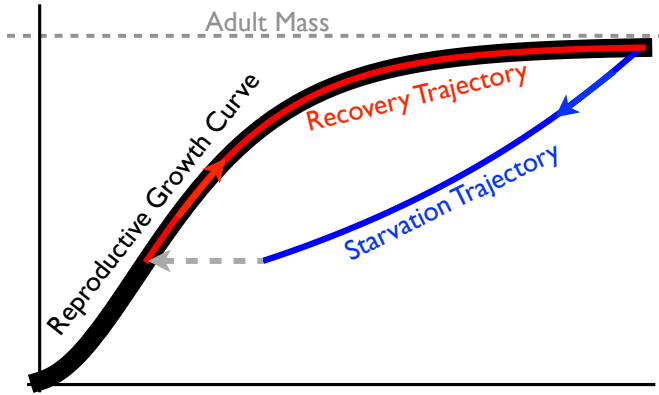


Fig. 1: The growth trajectory over absolute time of an individual organism as a function of body mass. Initial growth follows the red trajectory to an energetically replete adult mass M . Starvation follows the concave blue trajectory to $m_{\text{starve}} < M$, whereas recovery follows the convex growth trajectory from m_σ to M .

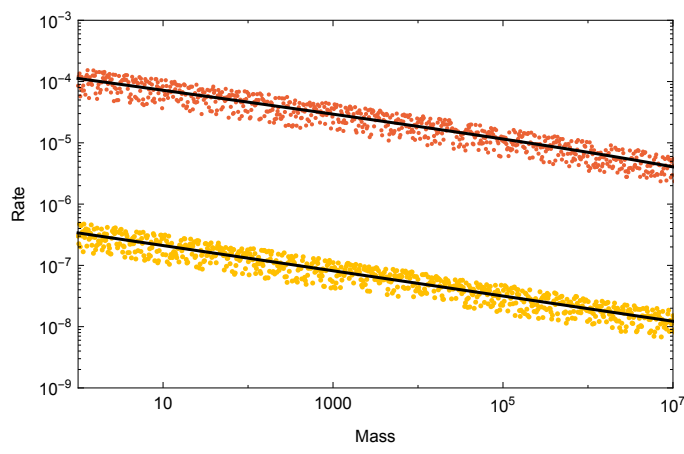


Fig. 2: Allometrically constrained starvation rate σ (red) vs. reproductive rate λ (yellow) as a function of mass M . The rate of starvation is greater than the rate of reproduction for all realized terrestrial endotherm body sizes. Each data point is determined by fixing the mass M and then choosing parameters in a $\pm 20\%$ range about the allometric values.

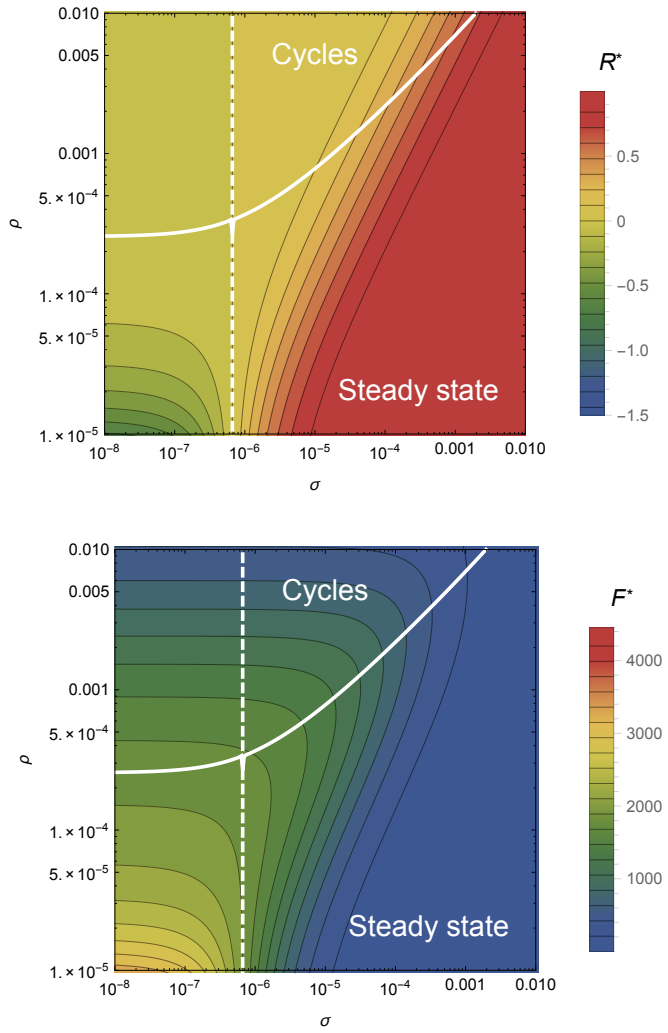


Fig. 3: The transcritical (dashed) and Hopf bifurcation (solid) as a function of the starvation rate σ and recovery rate ρ . These bifurcation conditions separate parameter space into infeasible, cyclic, and steady state dynamic regimes. The color gradient shows the steady state densities for (A) the resource R^* and the (B) energetically replete consumers F^* , (warmer colors denote higher densities). Steady state densities for the energetically deficient consumers H^* (not shown) closely mirror those for F^* .

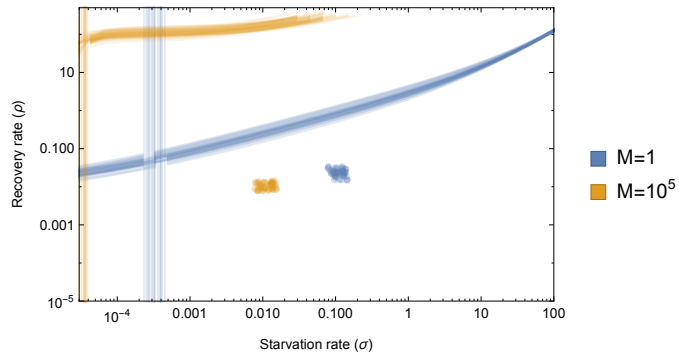


Fig. 4: Transcritical (vertical lines) and Hopf bifurcations (curves) with allometrically determined starvation σ and recovery ρ rates as a function of minimum and maximum mammalian body sizes: 1 gram (blue) and 10^7 grams (orange), respectively. Replicates show the role of the 20% variation about the mean allometric parameters, which influences both the energetic rates as well as the position of the TC and Hopf bifurcations.

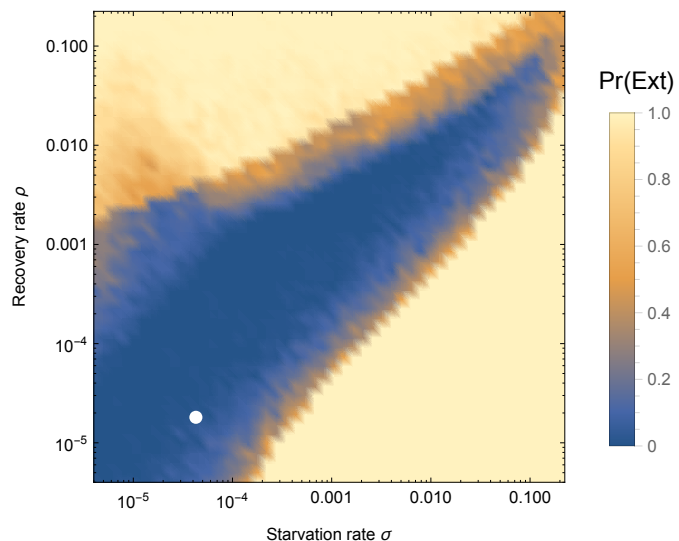


Fig. 5: Probability of extinction for 1000 consumer population trajectories as a function of σ/ρ for initial densities $A(F^*, H^*, R^*)$, with A a random uniform variable in $[0, 2]$. Extinction is defined as the population trajectory going below $0.2 \times$ the allometrically constrained steady state at any time between 10^2 and $\leq 10^6$. [Insert a distribution instead of a scatter plot above the main panel and describe it precisely] The values above the extinction plot are the allometrically constrained σ/ρ with 20% variation around the mean.

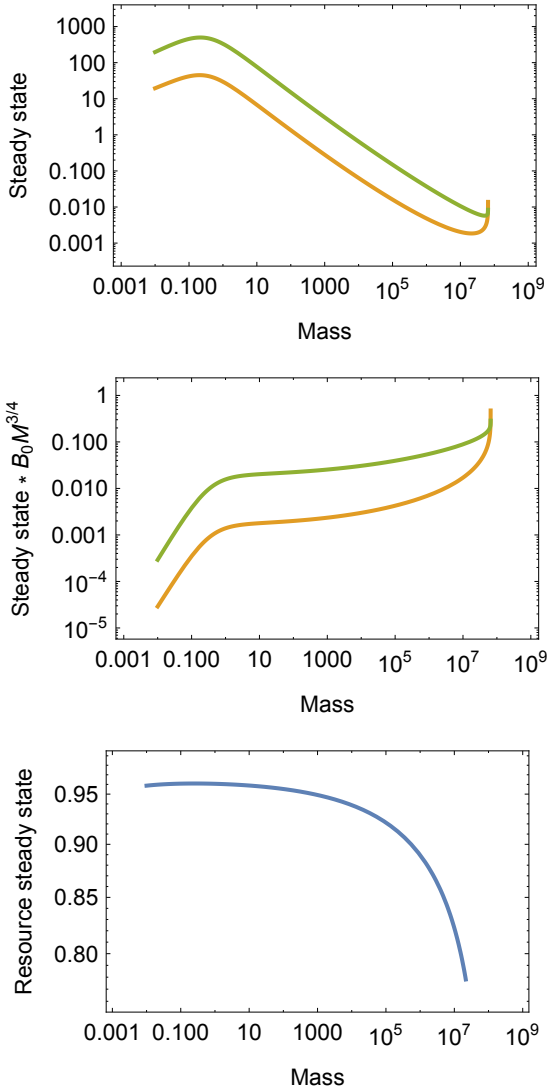


Fig. 6: (A) Consumer steady states F^* and H^* as a function of body size. Energetic rates as a function of body size, with the ratio σ/ρ (B) and both σ (red) and ρ (purple; C) drawn separately with 20% variation around the mean. Steady state densities decline sharply at $M = M_{\min}$ due to the precipitous decrease in the recovery rate. The minimum mammalian body mass (Etruscan shrew) is denoted by the orange shaded region that coincides with the decline of the recovery rate.

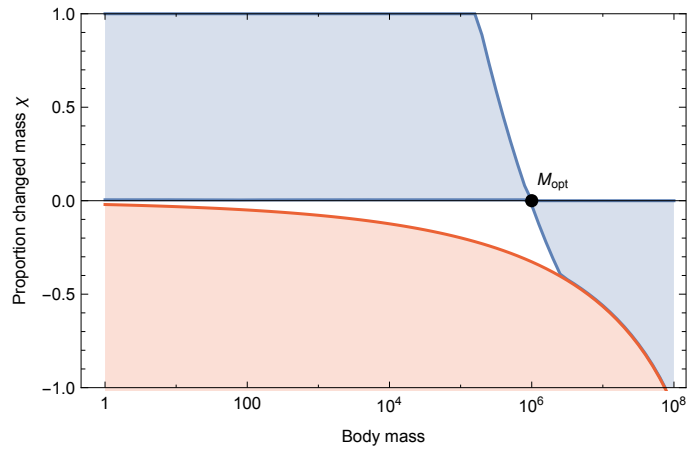


Fig. 7: Invasion feasibility for organisms with a proportional change in mass χ against a population with a resident body mass M . The blue region denotes values of χ that result in successful invasion. The red region denotes values of χ that result in a mass that is below the starvation threshold and is thus infeasible.